I.J. Image, Graphics and Signal Processing, **2022, 1, 40-49**
Published Online February 2022 in MECS (http://www.mecs-press.org/)
DOI: 10.5815/ijigsp.2022.01.04

Digital Method of Automated Non-destructive Diagnostics for High-power Magnetron Resonator Blocks

Serge Olszewski
Taras Shevchenko National University of Kyiv, Ukraine
E-mail: solaristics@gmail.com

Yaroslav Tanasiichuk
Taras Shevchenko National University of Kyiv, Ukraine
E-mail: tanasiichuk9247@gmail.com

Viktor Mashkov
University of J.E. Purkyne in Usti nad Labem, Czech Republic
E-mail: viktor.mashkov@ujep.cz

Volodymyr Lytvynenko
Kherson National Technical University, Ukraine
E-mail: immun56@gmail.com

Irina Lurie
Kherson National Technical University, Ukraine
E-mail: lurieira@gmail.com

Received: 17 October 2021; Accepted: 06 December 2021; Published: 08 February 2022

Abstract: The paper reveals the problem of the lack of standard non-destructive diagnostic methods for high-power microwave devices aimed at regeneration. The issue is understudied and requires further research. The conducted analysis of state of the art on the subject area exhibited that image processing was used to specify the examined object's target characteristics in a wide range of research. Having summarized the considered image comparison methods on the subject area of this work, the authors formulated several requirements for the selected image analysis method based on the automated non-destructive diagnosis of resonator units for high-power magnetrons. The primary requirement is using non-iterative algorithms; the second condition is a chosen method of image analysis, and the third option is the number of pixels for a processed image. It must significantly exceed the number of descriptors required for making a decision. Guided by the analysis results and based on the results of previous studies conducted by the authors, the algorithm for identifying a defect in the resonator unit of a microwave device based on the image of the frequency-azimuthal distribution for the probing field phase difference expressed by the Zernike moments is proposed. MATLAB R14a was used as a modeling environment. The descriptor vector was restricted to the Zernike moments, including the 7th order. The work is interdisciplinary and written at the intersection of technical diagnostics, microwave engineering, and digital image processing.

Index Terms: Technical diagnostics, non-destructive diagnostic methods, regeneration, digital image processing, the Zernike moments, defect, microwave engineering.

1. Introduction

Powerful electron-vacuum VHF devices with expired lifetime can be recovered for reuse by relatively inexpensive replacement of relevant components. To diagnose the inner state of such devices, it is crucial to avoid technological operations, including dismantling devices for their visual inspection. This diagnosis aims at determining whether it is possible to provide the reusability of such devices. It looks essential to perform the diagnosis automatically at the initial technological stages of mass recycling and recovery of these devices. This automation will eliminate unskilled manual

labor at the scenes of sifting out those devices that cannot be recovered and are subject to disposal. Such automation is impossible without making the necessary structural changes in the UHF devices. However, the nature of these changes is determined by the specifics of the selected diagnostic technique for such devices. The proposed work considers the possibility of atypical digital image analysis methods for automated identification of the response of high-power magnetron resonator units to the probing signal.

As a valuable research result, it should be noted that it is possible to represent and deliver the prepared image of the frequency-azimuthal distribution for the probing microwave field phase difference by the Zernike moments of the seventh order or less. This allows a complete system of 5-dimensional descriptor vectors to be formed. Such image representation of the frequency-azimuthal distribution of the phase difference for the probing microwave field is used to detect parasitic sputtering with constant physical and geometrical characteristics on a working surface of the resonator unit and for their localization.

The main contributions of the manuscript are:

1. The proposed approach is based on object orientation how to perform a streaming algorithm for analysis of the graphical representation of the phase structure for the probing VHF field in a resonator unit of electron-vacuum sources of powerful electromagnetic radiation for solving an issue of the automated decision for their suitability in the subsequent regeneration. An image analysis model is based on a two-dimensional circular grid. Target decision making is reduced to a correlational comparison of the reference and test vectors for the descriptors.
2. The system of 6-dimensional vector descriptors is developed based on the computation of the Zernike moments for a graphical representation of the azimuthal-frequency phase distributions of the UHF field in the resonator block of a powerful magnetron, which allows detecting and localizing the spurious sputtering on working surfaces of a device.
3. A software system for automated non-destructive real-time diagnostics of high-power UHF devices for further regeneration is implemented.

Thus, the critical issue is improving the renewal's production cycle for powerful electron-vacuum devices with expired lifetime. The problem's solution focuses on improving the quality and productivity of automated control systems by improving the algorithms and using the information system designed to solve the diagnostic tasks of post-operational defects of powerful electron-vacuum low-frequency devices.

In this regard, the section Related Works is devoted to choosing the most appropriate algorithm for image analysis.

The section Problem statement describes the problem of developing a streaming algorithm for extraction and processing image descriptors for automated identification of the resonator units' response for high-power magnetrons to the probing signal to diagnose them. To solve this problem in the section Materials and Methods, a block diagram of the algorithm for identifying a defect in the resonator unit of a microwave device on an image of the frequency-azimuthal distribution for the probing field phase difference description, and the used mathematical tools are described in detail.

The experimental study was carried out according to the proposed algorithm. This study is described in the section Experiment. The section Results and Discussion is devoted to assessing the results of the NSRU-diagram image transformation and the response analysis of descriptor vectors to a defect's position in the device structure. The section Conclusions summarizes the obtained results and outlines the further improvement of the proposed method for non-destructive diagnosis of microwave devices.

2. Related Works

Digital image processing as a method of determining the target characteristics of the studied object is used in a wide range of research areas. For example, in [1,], the analysis of satellite photographs for seismic anomaly prediction was used. In work [2], the authors use image analysis methods of mammograms to diagnose oncological diseases. And the nature of image analysis methods can be oriented both to the specifics of digital image acquisition hardware [3] and to machine methods of analysis and extraction of comparative features from ready digital images [4-8].

The authors of [1] apply an image processing approach to extract preliminary seismic features to identify an impending earthquake (EQ). For this purpose, they have developed an algorithm using "Color Histogram-based Search and Extraction Technology." The proposed image processing technique (IPT) is a -well-known approach for extracting information from different image shades. Research [1] shows that the IPT technique deserves significant attention with applications in remote atmospheric management, sensing, medical imaging, forensics, materials science, military science, and pattern recognition.

As a rule, the images of the examined sample with the reference image are used to identify target features. The authors of [4] carried out a detailed analysis of modern machine methods and tools used for image comparison. Among the simplest and most conspicuous ways, they refer to the sequential comparison of pixels. The mechanism of this method compares the color of pixels having the exact coordinates within the reference and working image. If the color of each pixel of both images is the same, then the two images are identical.

If the mechanism of pixel comparison is supplemented with such parameters as "Pixel Tolerance," "Color Tolerance," and "Transparent Color," defining the value of each of the parameters allow you to process bitmap images

more flexibly. So "Pixel Tolerance" defines the allowable number of heterogeneous pixels. If the number of different pixels is less than or equal to Pixel Tolerance, the comparison engine considers the images identical.

"Color Tolerance" defines the allowable color difference at which two pixels should be treated as identical. The acceptable color difference for each RGB component of the compared pixels is an integer value in the range 0-255. Two pixels are considered equivalent if the difference between the intensities of each of their color components does not exceed the specified value.

The "Transparent Color" option allows you to reduce the number of pixels compared. If you set the RGB component value for this parameter, all pixels with similar deals in the base image are excluded from the comparison procedure. For example, if "Transparent Color" is grey, then all grey pixels in the reference image will correspond to any color with the exact coordinates in the working image.

As the authors of [4] claim, the simplicity and reliability of the pixel comparison method for high-resolution images do not compensate for its computational resource-intensiveness. The main drawback of the process is its intense sensitivity to affine transformations and changes in the scale of the working image concerning the reference image. Thus, a slight displacement or rotation of the operating image concerning the reference image causes the method to show a negative comparison result for completely identical photos. Such an approach recalls the technique described in [5].

Other deterministic image comparison methods considered by the authors of this paper, such as the Hausdorff distance comparison, aim to find differences in images rather than determine a measure of their similarity.

The Hausdorff distance measures the degree to which each point in the model set lies next to some point in the image set and vice versa. Algorithms for calculating the Hausdorff distance between all possible relative positions of the working and reference images are presented. At insignificant displacements of the working image close to the reference image, they give the obtained results minor deviations. However, calculating the Hausdorff distance differs from many other shape comparison methods in that no correspondence is established between the model and the image.

A statistical comparison of images is adequate for analyzing experimental data. The tools used for such image comparison are often based on multivariate statistics and use the images as an ensemble of observations. So one method of image comparison is to model the images by random Gibbs fields with a finite number of parameters and check the equality of parameters between the merged images of each group. We obtain the minor statistic that is easy to compute, and the asymptotic distribution of the statistic is the χ^2 – distribution [4].

For making a target decision when determining the degree of similarity between the reference and working images, it is often enough to determine the identity of a sufficiently small number of distinct image segments. Image segmentation methods are used to solve such problems at preliminary data preparation.

The image is usually converted into segments or areas. It is assumed that these areas are connected and represent a set of homogeneous pixels. That said, different methods for identifying such areas are quite often assigned to the same group of scenarios, even if the result and the information they provide are very different. This applies, for example, to edge detection methods, image clustering, and threshold algorithms, all of which are classified as "image segmentation procedures" despite apparent differences in their results.

There is a significant difference between image classification methods, edge detection methods, image segmentation methods, and hierarchical image segmentation methods. Notably, in addition to the close relationship between them, these methods address different objectives and produce different results. In the article [5], the authors give a detailed conceptual analysis of such methods. The results of this analysis help determine the scope of applicability of a particular method. For example, they perform classification, detection, segmentation, or hierarchical segmentation.

Another approach adopted in image processing is image segmentation and feature extraction and classification [7]. The distinguishing feature of such image segmentation is object-oriented rather than pixel-based analysis.

In [7], the authors propose an effective image segmentation method that considers high-resolution panoramic images' spatial and spectral information. The procedure is based on multispectral nonlinear boundary preservation, smoothing, and extraction of multispectral boundary, which is used as valuable information for image segmentation. In the proposed way, the authors use the integration of multispectral and gradient information available in the image to provide the homogeneity of the image region with precise and closed boundaries.

Feature extraction based on image texture is another method of evaluating target characteristics. In [8], the authors state that the image classification process is best. It involves GLCM statistical matrix, structure, wavelet, and texture features based on adequate models. Statistical and wavelet-based texture features are most commonly used for an image-based object classification system. Texture features can be used to recognize both the external properties of objects under study and the internal characteristics associated with the manifestation of texture [8].

Generalization of the considered methods for image comparison related to the subject area of this work makes it possible to formulate several requirements for the selected method of image analysis put in the basis of the automated non-destructive diagnostics of resonator units for high-power magnetrons:

1. The diagnostic results of the investigated object should be presented in the form of an image convenient for machine analysis.

2. The image analysis method should be insensitive to scale and affine transformations of the image.
3. The analysis method should be weakly sensitive to stochastic image distortions.
4. The number of descriptors extracted from the image should be minimally sufficient to make a target diagnostic decision.

3. Problem Statement

The digital method of image analysis applied for automated identification of the high-power magnetron resonator units' response to a probing signal is intended to be used in real-time. Therefore, the required method should not be based on iterative algorithms. In this case, the pixels' number of the processed image should significantly exceed the number of descriptors for making a decision. Thus, developing an appropriate streaming algorithm for extracting and processing a relatively small number of descriptors seems relevant enough.

A mathematical model used for solving the diagnostic problem is formulated as follows: based on a geometric shape of a resonator unit in an electron-vacuum device and the experimental value of the UHF field amplitude at control points, it is required to compute the frequency-space distribution of the field phase $\Phi(\varphi,\omega)$ and obtain its image in polar coordinates. This paper used frequency ω as the radial coordinate r, an azimuthal angle φ as the azimuthal coordinate φ, and gray intensity $I(r,\varphi)$ as a value of the electromagnetic field phase overrun $\Phi(\omega,\varphi)$ to represent the spatial frequency distributions for the UHF field graphically. Constructing the descriptor vectors $\vec{\mathbf{D}} = (D_1, D_2, \ldots, D_i, \ldots, D_N)^T$ was performed by computing the Zernike moments of the *i*th order. The decision on the presence and localization of the defect was driven by estimating the Pearson's coefficient of mutual correlation between the testing vector $\vec{\mathbf{D}}$ and a reference descriptor vector $\vec{\mathbf{S}}$ of the descriptors:

$$\eta = \frac{\sum_{i=1}^{N}\left(D_i - \bar{D}_i\right)\left(S_i - \bar{S}_i\right)}{\sqrt{\sum_{i=1}^{N}\left(D_i - \bar{D}_i\right)^2 \sum_{i=1}^{N}\left(S_i - \bar{S}_i\right)^2}}$$

and by checking its closeness to "1". Here $\bar{D}_i$ and $\bar{S}_i$ signify the arithmetic mean of the descriptors' coordinates. The proposed similarity measure of the descriptor vectors is used as a condition for decision making. It is the most straightforward measure but not the only possible one. Mathematical methods for comparing descriptor vectors are developed for a reliable automated decision-making system.

4. Materials and Methods

One of the diagnostic methods of the resonant elements' state for powerful electron-vacuum VHF devices is the method that consists in excitation of the VHF field in a working area of these devices in a frequency band exceeding a resonance value. These diagnostics were applied to the magnetron and described in [10,11]. Let us call it the non-resonant sounding of resonator blocks (the NSRU-methodology), and let us call the results' graphical expression of this probing to be an NSRU-diagram.

The measurement result obtained by applying the method is graphically exemplified as a pie diagram describing the frequency-azimuth distribution of the phase difference for a probing field between an excitation point and an arbitrary point in the cavity of the magnetron's resonator unit in Fig.1. According to this method, these points are picked on a circle passing through an excitation point of the field [12,13]. The center of this circle lies on the symmetry axis of a magnetron's resonator unit [14,15].

The probing field's frequency is plotted along the chart's radius. For the investigations described in [10, 11], the probing field's frequency was chosen in the range of 7 to 20 GHz. The azimuth angle of the diagram corresponds to the arc length of the circle between the excitation point of the VHF field and the registration point of the probing signal. The intensity of the chart's filling corresponds to a phase difference value in the range from - 180 °to +180 °.

As can be assumed from the graphs mentioned above, the method is sensitive to the presence of a defect in the resonator system of a device under examination. It is noticed as a change in the structure of the chart's image. Accordingly, Fig.1(b), which corresponds to the faulty device, contains a more extensive number of structural elements compared to those on the diagram (Fig.1(a)). In Fig. 1(a), the graph presents the diagnostic result for the device free of defects.

However, visual analysis of these images for the defect's localization is tricky. Moreover, the requirements to lower the cost of the described diagnostics method are apparent. Costly and unproductive human work should be replaced by automatic image analysis and comparison methods.

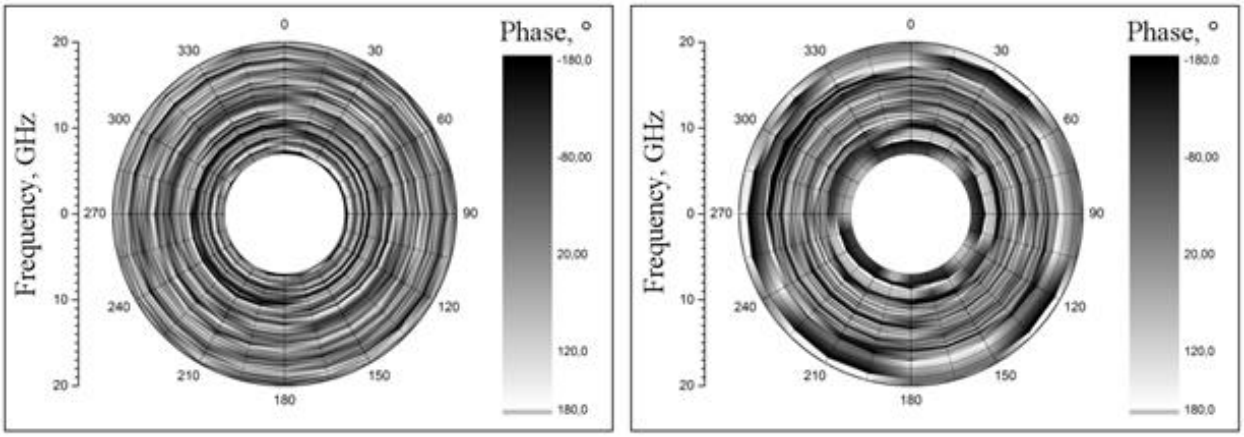

(a) (b)

Fig. 1. The frequency-azimuthal distribution of the UHF field phase difference in the magnetron's resonator unit cavity. Diagram (a) corresponds to the case when the defect is absent; diagram (b) corresponds to the defect's presence.

The streaming algorithm for the defect's identification in the UHF-device resonator block based on the image of the frequency-azimuth distribution for the probing field phase difference based on the NSRU–diagnostic methodology is presented by a scheme in Fig.2.

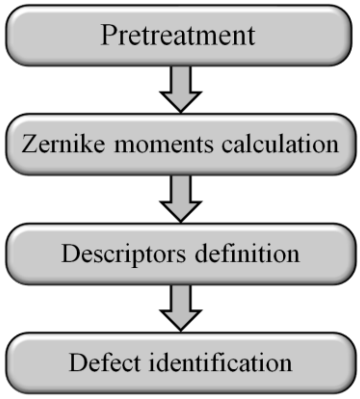

Fig. 2. The defect identification algorithm at the UHF device's resonator block is based on the image of the frequency-azimuthal distribution for the probing field phase difference.

At the "**Pretreatment**" stage, the frequency-azimuth distribution's images are prepared, transforming them into a more acceptable form for decomposition by the circular Zernike polynomials [16-19]. The outcomes' picture of the NSRU-method has a form of a ring with a monotone inner region. Moreover, the response of the probing field to the defect reflected by the structural elements' growth in the image is localized in two circular areas that constitute ~30% of the total area. The Pretreatment step that eliminates the drawbacks of the NSRU-diagrams projects the ring region onto the circular part. Coordinates of the image's elements are transformed using the formulas:

$$\begin{cases} \vartheta' = \vartheta, \\ r' = R + \frac{R}{\Delta R}(r - R) \end{cases} \tag{1}$$

where $R = \frac{F_{max}}{F_{\text{res}}}$ and $\Delta R = \left(F_{\max} - F_{\min}\right)/F_{\text{res}}$.

where F_{max} and F_{min} mark up the maximum and minimum frequencies of the probing UHF–field; F_{res} is a resonant frequency of a resonator block.

At the next stage of the algorithm, calculations of the Zernike moments [11, 16-18] are performed for a discrete pixel size image. The estimates are carried out according to the formula:

$$Z_{\varphi\eta} = \frac{p+1}{n}\sum_i^N \sum_k^M V_{\varphi\eta}(r_{ik}, \vartheta_{ik}) f(x_i, y_k) \tag{2}$$

where $f(x_i, y_k)$ stands for an experimental image; r_{ik}, ϑ_{ik} are discrete polar coordinates:

$$\begin{cases} r_{ik} = \sqrt{x_i^2 + y_k^2}, \\ \vartheta_{ik} = arctg\frac{y_k}{x_i}, \end{cases} \text{ provided that } r_{ik} \le 1, \tag{3}$$

$V_{\varphi\eta}(r,\vartheta) = R_{\varphi\eta}(r)e^{-j\eta\vartheta}$ is a family of the orthogonal Zernike polynomials defined on the single circle where

$$R_{\varphi\eta}(r) = \sum_{k=0}^{\frac{(\varphi-\eta)}{2}} \frac{(-1)^k(n-k)!}{k!\left(\frac{(\varphi+\eta)}{2}-k\right)!\left(\frac{(\varphi-\eta)}{2}-k\right)!} r^{\varphi-2k}. \tag{4}$$

As the ordering of the Zernike moments $\varphi + \eta$ increases, a dynamic range of their values proliferates. This makes it very difficult to analyze the shape of their shell. At the same time, the Zernike moments' shell for the NSRU-diagrams indicates the defect's presence and its localization on the working surfaces in the resonator unit.

At the "**Descriptors' definition**" step, the values $Z_{\varphi\eta}$ are recomputed (presented) into a more convenient form for the analysis: $A_{\varphi\eta} = \left|log\left(\left|Z_{\varphi\eta}\right|\right)\right|$ (the so-called "**given Zernike moments.**") Also, at this stage, components of the descriptor vector $\vec{\boldsymbol{D}} = \left(D_{11}, \dots, D_{1\eta}, \dots, D_{1J}, \dots, D_{\varphi 1}, \dots, D_{\varphi\eta}, \dots, D_{I,J}\right)^T$, $\varphi = \overline{1,I}$, $\eta = \overline{1,J}$ are determined. Based on this vector, decision-making on the defect's presence in the resonator unit and its localization can be made. A dimension of the descriptor vector $K = I + J$ is defined as a minimum order of the Zernike moments to be sufficient for the defect's localization. When performing the defect's localization (in actual resonant blocks), it is assumed that the defects expressed in the form of parasitic sputtering have a finite discrete set of position values $\mathbb{L}$. The components of the descriptor vector are determined by:

$$D_{\varphi\eta} = \frac{\left(A^0_{\varphi\eta} - A_{\varphi_\eta}\right)}{max\left\{A^0_{\varphi\eta} - A_{\varphi_\eta}\right\}} \tag{5}$$

where $A^0_{\varphi\eta}$ is the reduced Zernike moments for the NSRU–diagram in a device without faults. In any case, a dimension of the descriptive vector K depends on the geometric size of the set $\mathbb{L}$ and, in most cases, is less than a number of pixels in the NSRU-diagram image.

At the step "**Defect's identification**," a comparison of the reference descriptor vector $\vec{\boldsymbol{D}}_{pattern}$ with the vector $\vec{\boldsymbol{D}}$ is obtained. This comparison should be performed employing appropriate statistical methods or classification algorithms. The components' values of the vector $\vec{\boldsymbol{D}}$ may depend on many unaccounted physical characteristics of the defect, and in a general case, are random values. However, choosing the most appropriate comparison method is a subject of independent research and is beyond the paper's scope.

5. Experiment

The data obtained in [9, 10] were used to examine every stage of the proposed streaming algorithm. For this purpose, the pie-chart image without the applied graduation grid and captions was taken (Fig. 3).

The image size was 470×470 pixels. The algorithm was tested on eight images of the NSRU diagrams corresponding to different defect positions on the working surface of the magnetron resonator unit and the magnetron's diagram without flaws.

Fig. 3. An initial image of the NSRU-diagram for checking the streaming algorithm.

The physical and geometric characteristics of the defect in all positions were left unchanged. Every step of the algorithm was performed in the MATLAB R14a environment.

The descriptor vector was restricted to the Zernike moments, including the 7th order. In Table 1, the assessment results of the execution time for the streaming algorithm are given.

Table 1. Execution time of the streaming algorithm.

Function Name	Calls	Total Time	Self-Time*	Total Time Plot (dark band = self time)
Mol_trans	1	35.628 s	0.806 s	
Mol_trans>invmoments	10	19.122 s	0.372 s	
Mol_trans>compute_m	10	18.685 s	18.211 s	
xlswrite	1	12.482 s	0.140 s	
actxserver	1	6.624 s	6.624 s	
xlswrite>ExecuteWrite	1	5.549 s	1.362 s	
iofun\private\openExelWorkbook	1	2.844 s	2.745 s	
subplot	1	1.584 s	1.514 s	
imread	9	1.309 s	0.128 s	

* Self-time is the time spent in a function, excluding the time spent in its child functions. Self-time also includes overhead resulting from the process of profiling.

MATLAB built-in functions generated the table. Assessment of the execution time showed that the total execution time of the algorithm is ~36 sec. Writing data to a file takes approximately12 sec.

The time for descriptor calculation per image is equal to 2 sec. This is commensurate with the ordinary time of measurement and formation of the NSRU– diagram. An order of magnitude can reduce this time if modern controllers form the descriptor vector. Thus, examination of the proposed streaming algorithm on actual objects has proved its ability to be used in automated diagnostic systems of powerful low-frequency devices by the NSRU-method.

6. Results and Discussion

The results of the NSRU-diagram image transformation performed in the preprocessing stage are demonstrated in Fig. 4.

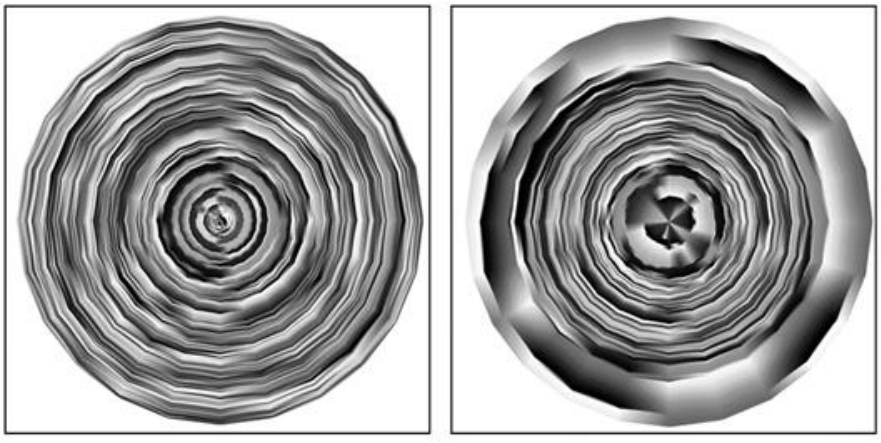

(a) (b)

Fig. 4. Transformed NSRU–diagrams. Image (a) corresponds to the case when the defect is absent; image (b) corresponds to the defect's presence.

The figure displays the transformed images of NSRU diagrams for the case of the defect's absence in the resonator unit (Fig.4(a)) and the possibility of the defect's presence in one of the fixed positions (Fig.4(b)). The experiment demonstrated that the image's area disturbed by the defect's company had been increased up to 70% due to the preprocessing stage.

Consequently, preliminary preparation of an image for the Zernike moments' calculation significantly expands the image's area containing practical information.

The Zernike moments' estimation outcomes are illustrated in Fig.5 as the dependence of the moments' values on their order.

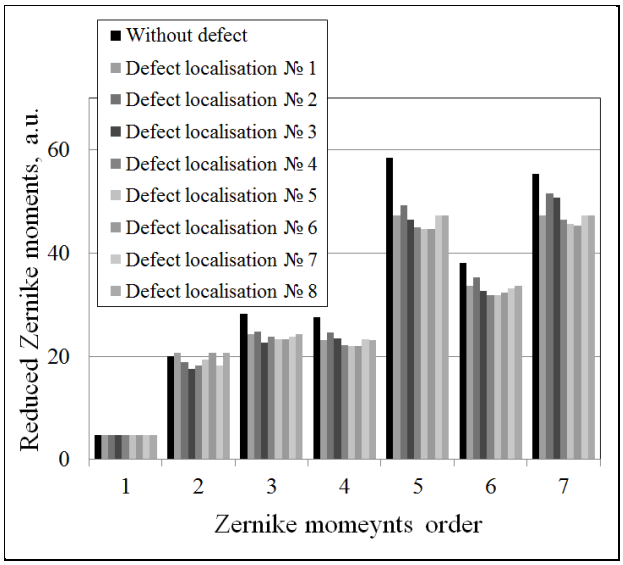

Fig. 5. Dependence of the reduced Zernike moments' values on the moments' order. The RZ-spectrum of black color corresponds to the case when the defect is absent, while the RZ-spectrum of gray shades corresponds to the point when the fault is present (at various positions).

Let us call such dependence the Reduced Zernike spectrum (the RZ-spectrum). The values marked in black correspond to the diagnosis result without a defect. Grey shades indicate the consequences related to the presence of a defect in the magnetron's resonator block at different fixed positions on the block's working surface.

As one can judge from the obtained dependence, the presence of defect changes values of the Zernike moments starting from the 2nd order. At the same time, starting from the 3rd order moments, values of the Zernike moments for all defect positions become smaller. The most considerable change occurs at the 5th order moment.

In addition to the overall reduction, a magnitude of the change in each component of the RZ spectrum responds differently to the defect's localization. The general decrease in energy of the RZ spectrum can be considered an indicator of a fault's presence. A shape of the spectrum displays information about the defect's localization.

A vector of descriptors $\vec{D}$ is more informative for automated decision-making regarding the defect's presence and location.

Its components are calculated in the third step of the streaming algorithm. The descriptor's dimensionality coincides with the maximal order of the calculated Zernike moments and equals 7.

The descriptor's components for various defect locations are presented in Fig.6.

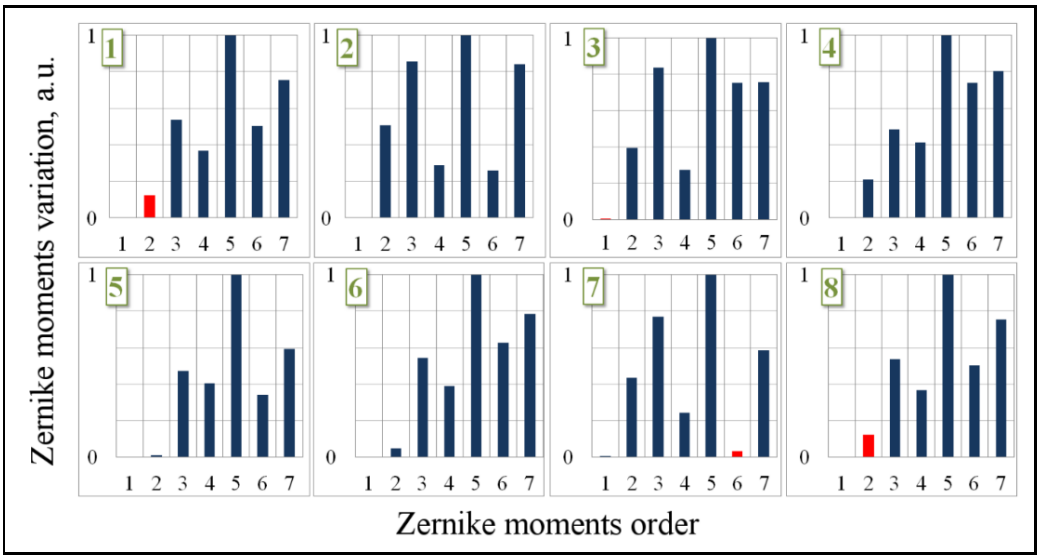

Fig. 6. Dependencies of descriptor vectors coordinate on a coordinate number at different defect locations on the working surface of the magnetron's resonator block.

The vector components are represented as a dependence of a coordinate value on a serial number. Positive elements of the descriptor vector are marked in blue and negative features are marked in red.

The abovementioned dependencies exemplify unambiguous correspondence of their form to the defect's location. The azimuthal symmetry of the magnetron's working surface coincides entirely with the descriptor vectors for the 1st and 8th defects areas.

Localization of the first defect corresponds to the location near an excitation point of the probing field to the left of the symmetry axis, and localization of the eighth defect corresponds to the area to the right. At these defect locations, the spatial distribution of the UHF field in the cavity of the magnetron resonator unit is mirror-like. At the same time, the Zernike moments are invariants of image rotations, and they do not distinguish mirror-like images.

Analysis of the descriptor vectors' response to the defect's location demonstrated that the descriptor's dimensionality could be reduced to 5. Since the first Zernike momentum does not feel completely the presence of a defect, where the fifth-order momentum always has a maximum value. Thus, in the streaming algorithm, to automate the technique of non-resonant probing for resonator units of powerful magnetrons, it turns out to be sufficient to compute the Zernike moments of the orders 2,3,4,6 and 7, which also leads to the computational time lowering.

Not to change the defect's physical and geometric characteristics, its identification step becomes trivial since it is diminished to calculating a difference between a reference 5-dimensional vector and the one under examination. Therefore, presenting its run results in this document is not advisable.

7. Conclusions

In this paper, we propose the streaming algorithm that automates the non-destructive diagnostics of high-power magnetron resonator units employing the method of non-resonant UHF-field probing. It is indicated that the representation of the prepared image for the frequency-azimuth distribution of the probing UHF-field phase difference by the Zernike moments is not higher than the 7th order. It allows forming a complete system of the 5-dimensional descriptor vectors. The generated system of the vectors allows specifying both the presence of parasitic sputtering with constant physical and geometrical characteristics on the resonator unit's operating surface and their localization.

As an expected further development of the proposed algorithm, the case of defects with arbitrary and unspecified physical and geometrical characteristics should be considered.

References

[1] S. Patgiri, M.Devi, A.K. Barbara, "Adaptation of Image Processing technique in identifying earthquake-induced anomalous feature from TEC: A New Approach," International Journal of Electronics and Applied Research (IJEAR), Vol.5, Iss.2, 2018.

[2] S.S. Ittannavar, R.H. Havaldar, B.P. Khot, "Comparative Assessment of Image Processing Techniques for the Early Detection of Breast Cancer: A Review," Biosci. Biotech. Res. Comm., Vol.13, No.13, pp.181-194, 2020.

[3] N. Jayanthi, S. Indu, "Comparison of Image Matching Techniques," International Journal of Latest Trends in Engineering and Technology, Vol.7, Iss.3, pp. 396-401, 2020.

[4] R. Katukam, P. Sindhoora, "Image Comparison Methods & Tools: A Review," the 1st National Conference on. Emerging Trends in Information Technology, pp. 35-42, 2015.

[5] V. Mashkov, "New approach to system-level self-diagnosis," Proc. of 11th IEEE International Conference on Computer and Information Technology (CIT 2011), pp. 579-584, 2011.

[6] C. Guada, D. Gomez, J.T. Rodriguez, J. Yocez, J. Montero, "Classifying image analysis techniques from their output," International Journal of Computational Intelligence Systems, Vol.9, pp. 43–68, 2016.

[7] Y.G. Byun, Y.K. Han, T.B. Chae, "A multispectral image segmentation approach for object-based image classification of high-resolution satellite imagery," KSCE Journal of Civil Engineering, Vol.17, No.2, pp. 486–497, 2013.

[8] P. Malkani, A. Sagar, K.R. Asha, A. Dubey, P. Singh, "An overview on crop - weed discrimination based on digital image processing using textural features," International Journal of Chemical Studies, Vol.7, No.6, pp. 2514-2520, 2019.

[9] M. Krishna, G. Satyanarayana, V. Devi Satya Sri, "Digital Image Processing Techniques in Character Recognition - A Survey," International Journal of Scientific Research in Computer Science, Engineering and Information Technology (IJSRCSEIT), Vol.2, Iss.6, pp. 2456-3307, 2017.

[10] S.V. Olszewski, Ya.V. Tanasiichuk, "Investigation of the influence of the defect in the magnetron resonator system on the parameters of its microwave field," Scientific notes of Tavrida National V.I. Vernadsky University Series: Engineering Sciences, Vol.31(70), No.5, pp. 43-48, 2020.

[11] S.V. Olszewski, Ya.V. Tanasiichuk, "The structural scheme synthesis of the system of test diagnostics of magnetron resonator blocks aimed to regeneration," Scientific notes of Tavrida National V.I. Vernadsky University Series: Engineering Sciences, Vol.32(71), No.1, pp. 28-32, 2021.

[12] P. Sumathi, S.Murugan, " GNVDF: A GPU-accelerated Novel Algorithm for Finding Frequent Patterns Using Vertical Data Format Approach and Jagged Array ", International Journal of Modern Education and Computer Science (IJMECS), Vol.13, No.4, pp. 28-41, 2021. DOI: 10.5815/ijmecs.2021.04.03.

[13] Hanan A. Al-Jubouri, " Integration Colour and Texture Features for Content-based Image Retrieval", International Journal of Modern Education and Computer Science (IJMECS), Vol.12, No.2, pp. 10-18, 2020. DOI: 10.5815/ijmecs.2020.02.02.

[14] Ye. Sulema, E. Kerre, O. Shkurat, " Vector Image Retrieval Methods Based on Fuzzy Patterns", International Journal of Modern Education and Computer Science (IJMECS), Vol.12, No.3, pp. 8-16, 2020. DOI: 10.5815/ijmecs.2020.03.02.

[15] U. Ali, S. Aftab, A. Iqbal, Z. Nawaz, M. Salman Bashir, M. Anwaar Saeed, " Software Defect Prediction Using Variant based Ensemble Learning and Feature Selection Techniques", International Journal of Modern Education and Computer Science (IJMECS), Vol.12, No.5, pp. 29-40, 2020. DOI: 10.5815/ijmecs.2020.05.03.

[16] Kh.M. Hosny, M.A. Hafez, "An Algorithm for Fast Computation of 3D Zernike Moments for Volumetric Images," Mathematical Problems in Engineering Volume, Article ID 353406, 17 p., 2012, doi:10.1155/2012/353406.
[17] A. Padilla-Vivanco, A. Martinez-Ramirez, F.-S. Granados-Agustin, "Digital image reconstruction using Zernike moments," Proc. SPIE 5237 Optics in Atmospheric Propagation and Adaptive Systems VI, 2004, DOI: 10.1117/12.514248.
[18] A. Gyrniak, E. Skubalska-Rafajlowicz, "Object Classification Using Sequences of Zernike Moments," 16th IFIP International Conference on Computer Information Systems and Industrial Management (CISIM), pp.99-109, 2017, 10.1007/978-3-319-59105-6_9. HAL-01656212.
[19] K.V. Kale, P.D. Deshmukh, S.V. Chavan, M.M. Kazi, Y.S. Rode, "Zernike Moment Feature Extraction for Handwritten Devanagari (Marathi) Compound Character Recognition," International Journal of Advanced Research in Artificial Intelligence (IJARAI), Vol.3, No.1, 2014.

Authors' Profiles

Serge Olszewski is an associate professor at the Faculty of Radio Physics, Electronics and Computer Systems, Taras Shevchenko National University of Kyiv. He received his Doctor of engineering sciences at the Faculty of Radio Physics, Electronics, and Computer Systems, Taras Shevchenko National University of Kyiv. His research interests include artificial intelligence and plasma physics.

Yaroslav Tanasiichuk received MSc. from the Radioelectronics Equipment, Systems, and Complexes degrees from the Radio Physics, Electronics and Computer Systems, Taras Shevchenko National University of Kyiv. He is currently pursuing his Ph.D. in Telecommunication at the Faculty of Radio Physics, Electronics, and Computer Systems, Taras Shevchenko National University of Kyiv. His research interest includes technical diagnostics and microwave engineering.

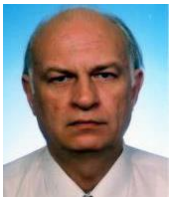

Viktor Mashkov is a Doctor of Science in Engineering, Docent in the IT Department at the University of J.E. Purkyne in Usti nad Labem, the Czech Republic. His primary research focuses on the dependability of computer systems, software fault tolerance, system-level self-diagnosis, and multi-agent systems.

Volodymyr Lytvynenko currently works at the Department of Informatics and Computer Sciences, Kherson National Technical University. He provides research in Data Mining, Computing in Mathematics, Natural Science, Engineering and Medicine, and Artificial Neural networks. His current research project is "Development of methods and algorithms for reverse engineering of gene regulatory networks based on soft computing."

Irina Lurie, Docent in the Department of Informatics and Computer Science, Kherson National Technical University, Kherson, Ukraine. Area of scientific interests: Inductive modeling of complex systems, computer intelligence systems, Development of hybrid algorithms

How to cite this paper: Serge Olszewski, Yaroslav Tanasiichuk, Viktor Mashkov, Volodymyr Lytvynenko, Irina Lurie, " Digital Method of Automated Non-destructive Diagnostics for High-power Magnetron Resonator Blocks", International Journal of Image, Graphics and Signal Processing(IJIGSP), Vol.14, No.1, pp. 40-49, 2022.DOI: 10.5815/ijigsp.2022.01.04

